

Dual-End Consistency Model

Linwei Dong^{1,2} Ruoyu Guo^{2†} Ge Bai² Zehuan Yuan² Yawei Luo^{1*} Changqing Zou^{1,3}

¹Zhejiang University ²Bytedance Inc. ³Zhejiang Lab

Abstract

The slow iterative sampling nature remains a major bottleneck for the practical deployment of diffusion and flow-based generative models. While consistency models (CMs) represent a state-of-the-art distillation-based approach for efficient generation, their large-scale application is still limited by two key issues: training instability and inflexible sampling. Existing methods seek to mitigate these problems through architectural adjustments or regularized objectives, yet overlook the critical reliance on trajectory selection. In this work, we first conduct an analysis on these two limitations: training instability originates from loss divergence induced by unstable self-supervised term, whereas sampling inflexibility arises from error accumulation. Based on these insights and analysis, we propose the **Dual-End Consistency Model (DE-CM)** that selects vital sub-trajectory clusters to achieve stable and effective training. DE-CM decomposes the PF-ODE trajectory and selects three critical sub-trajectories as optimization targets. Specifically, our approach leverages continuous-time CMs objectives to achieve few-step distillation and utilizes flow matching as a boundary regularizer to stabilize the training process. Furthermore, we propose a novel noise-to-noisy (N2N) mapping that can map noise to any point, thereby alleviating the error accumulation in the first step. Extensive experimental results show the effectiveness of our method: it achieves a state-of-the-art FID score of 1.70 in one-step generation on the ImageNet 256×256 dataset, outperforming existing CM-based one-step approaches.

1. Introduction

The rapid advancement of diffusion [18, 49, 52, 53] and flow-based [11, 28, 31] generative models has revolutionized data generation across image [42, 44, 65], 3D [30, 40, 58], audio [12, 29] and video generation [4, 56], yet their reliance on slow iterative sampling remains a fundamental bottleneck. While higher-order solvers [34, 35, 50]

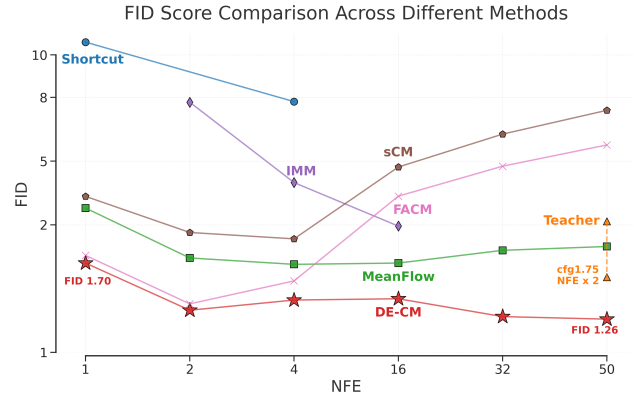


Figure 1. Comparison of FID scores across different models under various NFE settings, showing the superior performance of our method in both few-step and multi-step sampling.

offer limited acceleration, distillation techniques [48, 62, 63], particularly consistency models (CMs) [23, 54], have emerged as the most effective path toward few-step generation. CMs achieve efficient distillation by learning consistency function that directly maps noise to data along predefined trajectories. However, early discrete-time implementations suffered from discretization errors that potentially compromised output quality [14, 51], ultimately driving the development of continuous-time variants [33, 45].

Continuous-time CMs, while circumventing discrete error accumulation, do not address the fundamental limitations (including training instability and inflexible sampling) of CMs, thus impeding their wider deployment. Recent main efforts on stabilization, efficiency, and flexibility fall into three categories: 1) diffusion modeling. Methods like sCM [33] that employ TrigFlow to simplify the formulation of diffusion models, which unify the flow ODE and CMs. MeanFlow [15], AYF [45] and IMM [66] introduce the flow maps [5] to map noisy inputs directly to any point along the PF-ODE trajectory. 2) network architecture. Approaches [33] tailor the architecture design to achieve more stable and efficient training. 3) training objective with regularization. Approaches like IMM, MeanFlow, SplitMean-

*Corresponding Authors. † Project Leader.

Flow [16], sCoT [59] and FACM [39] reformulate the learning objective with additional constraints or flow modeling. While these efforts facilitate continuous-time CMs training, they remain fundamentally limited by treating suboptimal sub-trajectories as their optimization objectives. Methods like MeanFlow and AYF couple the optimization throughout the whole trajectories by learning mappings between any two points, as shown in Fig. 2 (a). These entangled learning objectives are particularly problematic given that CMs impose consistency as a network behavior property without an explicit boundary condition from the ground-truth flow characteristics, leading to slower convergence or even training collapse. Furthermore, approaches like sCMs treat vanilla CMs trajectory alone, potentially increasing instability due to the absence of the critical path. By explicitly decoupling the instantaneous velocity objective along the PF-ODE trajectory, FACM achieves improved training stability. This indicates that the core challenge lies in selecting the appropriate candidate trajectories to achieve both training stability and strong performance.

In this work, we begin with an analysis of two inherent limitations in vanilla CMs: unstable training and inflexible sampling. Our findings indicate that training instability arises from loss divergence, which is triggered by unstable self-supervised objectives and the catastrophic forgetting of original instantaneous velocity features. Furthermore, we attribute inflexible sampling to error accumulation caused by the the CMs sampler [23]. Based on these analysis, we propose a novel method, **Dual-End Consistency Model**, to achieve efficient, stable, and flexible model distillation under critical sub-trajectory clusters selection. We employ flow maps to incorporate entire transport space and identify the significant sub-trajectory clusters for optimization. Taking the intermediate time t as the dividing point, we focus on the following three trajectory segments: 1) Consistency Trajectory. 2) Instantaneous Trajectory. 3) Noise-to-Noisy Trajectory. The comparative illustration of our optimization trajectories is provided in Fig. 2. Consistency trajectories enable the model to perform inference over few-step via consistency property, while instantaneous trajectories serve as a boundary regularization to stabilize the training. By incorporating the noise-to-noisy trajectories, we formulate the training objective and leverage mix-sampler to alleviate the error accumulation imposed by the CMs sampler. DE-CM excels in few-step sampling on C2I and T2I tasks while maintaining performance across multi-steps. On ImageNet 256×256 [8], DE-CM achieves 1.70 FID using 1-NFE generation, as shown in Fig. 1.

The key contributions are summarized as follows:

- We analyze the potential constraints imposed on CMs and elucidate the underlying causes of instability and inflexible sampling.
- We propose DE-CM, a novel method for stable and effec-

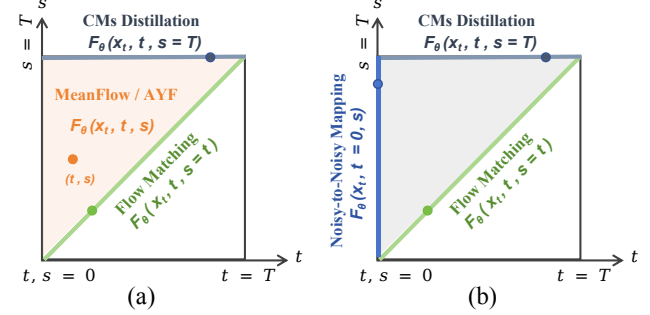


Figure 2. Comparison of learning objectives. (a): CMs Distillation [54] ($s = T$), Flow Matching [28] ($s = t$), MeanFlow [15] / AYF [45] (upper triangle). (b): DE-CM (triangular boundary).

tive training through the selection of vital trajectories.

- We derive a new objective noise-to-noisy mapping to learn a mapping from pure noise to arbitrary points.
- Our experiments on C2I and T2I demonstrate the effectiveness of DE-CM, achieving state-of-the-art performance on the ImagNet dataset with 250 training epoch.

2. Preliminaries

Diffusion Models and Flow Matching. Given a dataset with underlying distribution p_{data} and standard deviation σ , diffusion models learn to reverse a noising process that transforms a clean sample $x_1 \sim p_{data}$ into $x_t = \alpha_t x_1 + \sigma_t z$, where $z \sim \mathcal{N}(0, I)$, and the noise level increases as the timestep t decreases from T to 0. EDM [22] defines $\alpha_t = 1, \sigma_t = 1 - t$, and optimizes:

$$\mathbb{E}_{x_1, z, t} [w(t) \|f_\theta^{\text{DM}}(x_t, t) - x_1\|_2^2], \quad (1)$$

where $w(t)$ is the weighting and $f_\theta(x_t, t)$ is defined as:

$$f_\theta(x_t, t) = c_{\text{skip}}(t)x_t + c_{\text{out}}(t)F_\theta(c_{\text{in}}(t)x_t, c_{\text{noise}}(t)), \quad (2)$$

Here, F_θ is a neural network, and these terms $c(t)$ are scaling coefficients that stabilize training.

Flow matching (FM) uses differentiable schedules α_t, σ_t (e.g, $\alpha_t = t, \sigma_t = 1 - t$) and minimizes:

$$\mathbb{E}_{x_0, z, t} [w(t) \|F_\theta(x_t, t) - (\dot{\alpha}_t x_0 + \dot{\sigma}_t z)\|_2^2], \quad (3)$$

where $\dot{\alpha}_t$ and $\dot{\sigma}_t$ denote the derivatives with respect to t . Sampling solves the probability flow ODE (PF-ODE):

$$\frac{dx_t}{dt} = F_\theta(x_t, t), \quad (4)$$

from $x_0 \sim \mathcal{N}(0, I)$ at $t = 0$ to $t = 1$.

Consistency Models. Consistency Models (CMs) are designed to map any point x_t along a PF-ODE trajectory directly to its endpoint x_1 in a single step. This behavior is governed by a self-consistency property: for any pair of

points x_t and $x_{t'}$ on the same trajectory, the model must satisfy $f_\theta(x_t, t) = f_\theta(x_{t'}, t')$. This implies $f_\theta(x_t, t) = x_1$ for all $t \in [0, 1]$ with the boundary condition $f_\theta(x_1, 1) = x_1$.

Discrete-time CMs follow the Eq. (2) with $c_{skip}(1) = 1$, $c_{out}(1) = 0$ and learn the consistency between two adjacent timesteps. The training objective is defined as follows:

$$\mathbb{E}_{x_1 \sim p_{data}} [w(t) \cdot d(f_\theta(x_t, t), f_{\theta^-}(x_{t+\Delta t}, t + \Delta t))], \quad (5)$$

where $w(t)$ is the time-aware weighting, $\Delta t > 0$ is a minimal step, θ^- denotes $stopgrad(\theta)$ and $d(\cdot, \cdot)$ is a distance metric. Discrete-time CMs are sensitive to the discretization step size Δt , typically requiring carefully designed schedules to ensure convergence. Furthermore, the sample $x_{t+\Delta t}$ is commonly generated from x_t by numerically solving the PF-OFE process that introduces additional discretization error, potentially leading to suboptimal sample quality.

Continuous-time CMs avoid the accumulation of discrete errors by taking the limit $\Delta t \rightarrow 0$. When employing $d(x, y) = \|x - y\|_2^2$, the gradient of Eq. (5) converges to

$$\nabla_\theta \mathbb{E}_{x_t, t} \left[-w(t) f_\theta^\top(x_t, t) \frac{df_{\theta^-}(x_t, t)}{dt} \right], \quad (6)$$

where $\frac{df_{\theta^-}(x_t, t)}{dt} = \nabla_{x_t} f_{\theta^-}(x_t, t) \frac{dx_t}{dt} + \partial_t f_{\theta^-}(x_t, t)$ is the tangent of f_{θ^-} at (x_t, t) along the trajectory of the PF-ODE $\frac{dx_t}{dt}$ and $w(t)$ is the weighting function. This modeling approach eliminates the need for a predefined sampling interval Δt , thus avoiding discretization errors.

3. Limitations of Consistency Models

3.1. Training instability

Similar to discrete versions, continuous-time CMs face the challenge with training instability [14, 51]. To better understand the causes of instability, we analyze its ultimate training objective. Following the naive discrete-time CMs based on OT-FM, we set $c_{skip}(t) = 1$ and $c_{out}(t) = 1 - t$. Thus the training objective of Eq. (6) can be derived as follows:

$$\mathbb{E}_{x_t, t} [\|F_\theta(x_t, t) - F_{\theta^-}(x_t, t) + w'(t) \cdot g_{\theta^-}\|_2^2], \quad (7)$$

where $g_{\theta^-} = F_{\theta^-}(x_t, t) - v_\phi - (1 - t) \frac{dF_{\theta^-}(x_t, t)}{dt}$, v_ϕ denotes the desired trajectory tangent $\frac{dx}{dt}$ and it can be directly derived from data ($v_\phi = \dot{x}_1 + \dot{x}_0$) or predicted by a teacher model ($v_\phi = v_{\text{tea}}(x_t, t)$). ϵ is equal to Δt , $w'(t) = \frac{1}{2}w(t)\epsilon(1-t)$ and $w(t)$ is a custom weighting function with respect to t and commonly set to $\frac{1}{\epsilon}$ to accelerate convergence. To clearly delineate the training objectives, we further decompose Eq. (7):

$$\mathbb{E}_{x_t, t} [\|F_\theta(x_t, t) - v_\phi\|_2^2 + \|F_\theta(x_t, t) - \tilde{v}\|_2^2], \quad (8)$$

where $\tilde{v} = F_{\theta^-}(x_t, t) + (1 - t) \frac{dF_{\theta^-}}{dt}$. This formulation reveals that: 1) A divergence exists between the fully supervised and self-supervised components when F_θ has not converged. 2) The emphasis on consistency in F results in the

overshadowing of the pretrainind instantaneous velocity concept. These suggest inherent limitations in the optimization trajectory predefined by the vanilla CMs.

3.2. Inflexible Sampling Mechanism

CM sampling is constrained by the following two factors: 1) Inflexible sampling methods. The training of the CMs focuses solely on the mapping from any given point x_t to data point x_1 . This implies that any deviation in the initial data prediction propagates directly to the final output, leading to a complete failure. 2) Inflexible sampling steps. The model may exhibit artifacts due to error accumulation during multi-step sampling. CM sampling draws new noise for each noise addition process instead of reusing the initial noise (Using the initial noise leads to a significantly larger deviation from the trajectory [23, 54]), leading to error accumulation when injecting new noise. These two findings reveal that the suboptimal performance stems from the limitations of the CMs sampler.

4. Dual-End Consistency Model

MeanFlow [15] and AYF [45] indicate that the aforementioned limitation of CMs lies in the exclusive dependence on the time condition t , which is inherently insufficient to characterize the entire PF-ODE trajectory. Consequently, they augment the temporal specification with an auxiliary endpoint embedding s , enabling the estimation of the mean velocity along the trajectory. The trajectory consistency function is formulated as follows:

$$f_\theta(x_t, t, s) = x_t + (s - t)F_\theta(x_t, t, s) \quad (9)$$

where F_θ is a neural network. Eq. (9) encompasses the entire trajectories when given $t, s \in [0, 1]$ and $t < s$, thus satisfying both CMs and FM parameterization. This formulation will optimize any sub-trajectory defined by t and s and have access to ODE solver (e.g. Euler Sampler). However, unlike the consistency function that exhibits explicit boundary conditions $f_\theta(x_1, 1) = x_1$, the boundary conditions of Eq. (9) is not strictly constrained as t, s are both variables. This will introduces greater instability risks during training. Moreover, optimizing the entire sub-trajectory space also leads to inefficient training as the redundant trajectory optimization degenerates convergence. The computational complexity, $O(n^2)$, became a primary bottleneck, leading to slow optimization. Fortunately, we find that optimizing only specific sub-trajectory clusters is sufficient to ensure stable training and high-quality samples. We focus on three key trajectory clusters (Fig. 3): consistency trajectories, instantaneous trajectories and noise-to-noisy trajectories.

4.1. Few-Step Models with Consistency Trajectory

Given $t \in [0, 1]$ and $s = 1$, Eq. (9) can be equated to the consistency function of standard CMs. By analogy with the

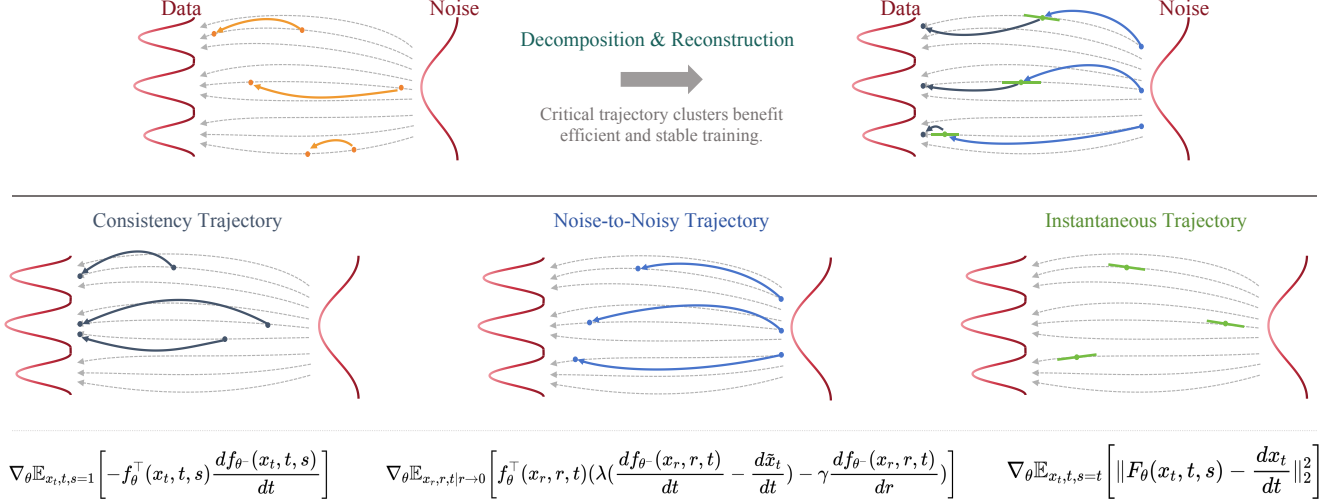


Figure 3. We select significant trajectories from the whole $\{(t, s) | t < s\}$ space and treat these selected trajectories as our optimization targets. Specifically, we employ the continuous-time consistency distillation trajectory to optimize the mapping from arbitrary time points to data, thereby achieving few-step distillation. We leverage the proposed noise-to-noisy (N2N) mapping objective to eliminate the constraint of predicting only x_1 points. We utilize flow matching loss to overcome the instability in training. We find that incorporating these three trajectory clusters is enough to enable stable and efficient optimization for few-step distillation.

derivation of Eq. (7), we can further simplify:

$$\mathcal{L}_{\text{cm}} = \mathbb{E}_{x_t, t, s|s=1} \left[\|F_{\theta}(x_t, t, s) - v_{\text{cm}}^{\text{tar}}\|_2^2 \right], \quad (10)$$

where $v_{\text{cm}}^{\text{tar}} = w'(t)\bar{v} + (1 - w'(t))F_{\theta-}(x_t, t, 1)$ and $\bar{v} = v_{\phi} + (1 - t)\frac{dF_{\theta-}(x_t, t, 1)}{dt}$. It can be seen that the final loss is a weighted combination of the model prediction and another velocity \bar{v} . Moreover, \bar{v} is defined as the instantaneous velocity $v_{\phi}(x_t, t)$ corrected by the average acceleration $\frac{dF_{\theta-}(x_t, t, 1)}{dt}$, thus representing the average velocity [15]. Given that $\frac{dF_{\theta-}(x_t, t, 1)}{dt}$ serves as the training objective but is not available in advance, the standard approach is to utilize Jacobian-Vector product (JVP) to dynamically compute it based on current neural network states. The total derivative, expanded via the chain rule, is:

$$\frac{dF_{\theta-}}{dt} = [\nabla_{x_t} F_{\theta-}, \frac{\partial F_{\theta-}}{\partial t}, \frac{\partial F_{\theta-}}{\partial s}] \cdot [v_{\phi}, 1, 0]^{\top}, \quad (11)$$

where $[v_{\phi}, 1, 0]$ is drawn from $[\frac{dx_t}{dt}, \frac{dt}{dt}, \frac{ds}{dt}]$, and $\frac{dx_t}{dt} = v_{\phi}$ represents the direction given by the pretrained diffusion or flow model along the PF-ODE. The consistency properties enable the model to learn the mapping from noisy input x_t to data x_1 . This is analogous to reflow that construct paired data, alleviating the difficulty of learning few-step models.

4.2. Flexible Models with Noise-to-Noisy Mapping

By optimizing the time interval $[0, t]$, we enable the model to map from pure noise x_0 to any intermediate noisy state x_t , rather than returning only to the data x_1 . To preserve the meaning of the random variable t , we reset the left endpoint

in Eq. (9) by $r \rightarrow 0$, while the right remains t . Following Eq. (5), for timestep t , under the L_2 norm, we have:

$$\mathbb{E}_{x_r, r, t|r \rightarrow 0} \left[w(r, t) \|f_{\theta}(x_r, r, t), \mathcal{S}_{\psi}(f_{\theta-}(x_r, r, t'))\|_2^2 \right], \quad (12)$$

where \mathcal{S}_{ψ} refers to *Euler Solver* on the PF-ODE starting from $x_{t'}$ to x_t ($t > t'$). Inspired by [45, 59], its gradient can be derived to converge to (See appendix)

$$\nabla_{\theta} \mathbb{E}_{x_r, r, t|r \rightarrow 0} \left[w(r, t)' f_{\theta}^{\top}(x_r, r, t) \left(\frac{df_{\theta-}(x_r, r, t)}{dt} - v_{\psi} \right) \right] \quad (13)$$

where $v_{\psi} = v_{\text{tea}}(f_{\theta-}(x_r, r, t), t)$ denotes the desired trajectory tangent $\frac{d\tilde{x}}{dt}$. Eq. (13) reveals the gradient convergence objective of the self-supervised loss Eq. (12) with respect to the right endpoint t . Considering the left endpoint r , we can regard it as a consistency function based on boundary $f_{\theta}(x_t, t, t) = x_t$. Then, its gradient objective can be derived from Eq. (6). The two optimization objectives can be expressed in weighted form, and their gradients can be proven to converge to (See appendix)

$$\nabla_{\theta} \mathbb{E}_{x_r, r, t|r \rightarrow 0} \left[w(r, t)' f_{\theta}^{\top}(x_r, r, t) \left(\lambda \frac{df_{\theta-}(x_r, r, t)}{dt} - \gamma \frac{df_{\theta-}(x_r, r, t)}{dr} - \lambda \cdot v_{\text{tea}}(f_{\theta-}(x_r, r, t), t) \right) \right], \quad (14)$$

where λ, γ are weighting factors. The final optimization loss \mathcal{L}_{n2n} can be expressed as:

$$\mathbb{E}_{x_r, r, t|r \rightarrow 0} \left[\|F_{\theta}(x_t, t, s) - F_{\theta-}(x_t, t, s) + w'(r, t)g\|_2^2 \right], \quad (15)$$

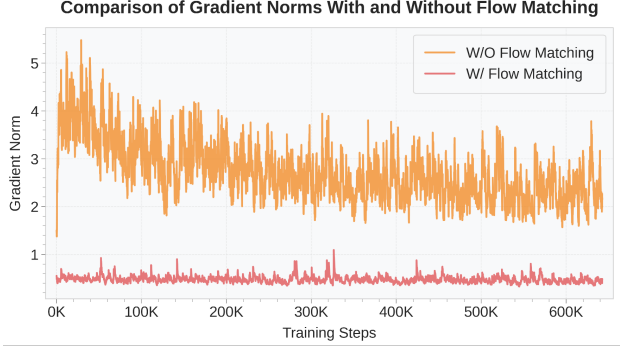


Figure 4. Comparison of gradient norm curves with and without flow matching boundary constraints.

where $g = (\lambda + \gamma)F_{\theta-} - (\gamma v_{\phi} + \lambda v_{\psi}) - (t - r)\dot{F}_{\theta-}$ and $\dot{F}_{\theta-} = [\nabla_{x_t}F_{\theta-}, \frac{\partial F_{\theta-}}{\partial t}, \frac{\partial F_{\theta-}}{\partial s}] \cdot [\lambda v_{\phi}, \lambda, -\gamma]^{\top}$. Eq. (15) utilizes the velocities on both sides of the endpoint r and t , along with the correction term from the neural network.

4.3. Stable Models with Instantaneous Velocity

Directly using Eq. (10) or Eq. (15) for optimization does not stabilize training. We find this is due to the absence of necessary boundary conditions. Following Eq. (8), We can restate the training objective when given t and s :

$$\mathbb{E}_{x_t, t, s} [\|F_{\theta}(x_t, t, s) - v_{\phi}\|_2^2 + \|F_{\theta}(x_t, t, s) - \tilde{v}\|_2^2], \quad (16)$$

where $\tilde{v} = F_{\theta-}(x_t, t, s) + (s - t)\frac{dF_{\theta-}}{dt}$. The dynamic calculation of $\frac{dF_{\theta-}}{dt}$ in Eq. (11) renders the self-supervised term susceptible to instability, which raises the risk that online models could diverge from a single erroneous update. The large gradient phenomena are shown in Fig. 4. However, when $s = t$, we observe that the original gradient update paradigm is driven solely by ground truth as the second term equals zero. This term also represents the left boundary condition. The single loss term makes the optimization objective deterministic, eliminating slack on the left-hand side. Similarly, for targets with loose right-hand constraints like Eq. (15), a right-hand regularization can be incorporated. This approach corresponds to selecting all instantaneous trajectory clusters and it makes training more stable (w/ flow in Fig. 4). The specific loss \mathcal{L}_{fm} is formulated as:

$$\mathbb{E}_{x_t, t, s|s=t} [\|F_{\theta}(x_t, t, s) - v_{\phi}\|_2^2 + L_{\text{cos}}(F_{\theta}(x_t, t, s), v_{\phi})], \quad (17)$$

Beyond its role as a robust regularizer, this loss function is designed to safeguard the pre-trained model’s capabilities, thus supporting multi-step ODE sampling.

The overall training process is shown in Algorithm 1.

4.4. Training Scheme

Adaptive Weighting. Following previous works [15, 39],

Algorithm 1: Training procedure

Input: Pretrained diffusion model F_{tea} , online model F_{θ} , paired dataset $\mathcal{D} = \{z_{\text{ref}}, y_{\text{ref}}\}$, loss metrics d_1, d_2, d_3 , hyperparameters $\lambda, \gamma, \eta, w_{\text{cfg}}, freq$, weighting function $w_1(t), w_2(r, t)$.

Output: Trained model F_{θ} .

// Initialize model

- $F_{\theta} \leftarrow \text{copyWeights}(F_{\text{tea}})$, $F_{\text{ema}} \leftarrow \text{copyWeights}(F_{\theta})$, $iters \leftarrow 0$
- while** $train$ **do**
- // Prepare Data
- Sample batch $z \sim \mathcal{N}(0, \mathbf{I})$ and $(z_{\text{ref}}, y_{\text{ref}}) \sim \mathcal{D}$
- Sample timestep $t \sim \mathcal{U}(0, 1)$
- $z_t \leftarrow (1 - t)z + tz_{\text{ref}}$
- $v_t^{\text{cond}} \leftarrow F_{\text{tea}}(z_t, t; y_{\text{ref}})$, $v_t^{\text{uncond}} \leftarrow F_{\text{tea}}(z_t, t; \phi)$
- $v_t \leftarrow v_t^{\text{cond}} + (w_{\text{cfg}} - 1) \frac{\eta(v_t^{\text{cond}} - v_t^{\text{uncond}})}{\|v_t^{\text{cond}} - v_t^{\text{uncond}}\|}$ // For from scratch, $v_t \leftarrow z_{\text{ref}} - z$
- // Continuous-time CD
- $F_{\text{cm}}, \nabla_t F_{\text{cm}} \leftarrow \text{JVP}(F_{\theta}, (x_t, t, 1; y_{\text{ref}}), (v_t, 1, 0))$
- $g_{\text{cm}} \leftarrow \text{sg}(F_{\text{cm}}) - v_t - (1 - t)\nabla_t F_{\text{cm}}$
- $v_{\text{cm}}^{\text{tar}} \leftarrow \text{sg}(F_{\text{cm}}) - w_1(t) \cdot g_{\text{cm}}$
- $L_{\text{cm}} \leftarrow d_1(F_{\text{cm}}, v_{\text{cm}}^{\text{tar}})$ // Eq. 10
- // Flow Matching
- $F_{\text{fm}} \leftarrow F_{\theta}(x_t, t, t; y_{\text{ref}})$
- $\mathcal{L}_{\text{fm}} \leftarrow d_2(F_{\text{fm}}, v_t)$ // Eq. 17
- $F_{\theta}, F_{\text{ema}} \leftarrow \text{update}(F_{\theta}, \mathcal{L}_{\text{cm}} + \mathcal{L}_{\text{fm}})$
- // Noise-to-Noisy Mapping
- if** $iters \% freq == 0$ **then**
- Sample time step $r \rightarrow 0$
- $z_r \leftarrow (1 - r)z + r z_{\text{ref}}$
- $v_r^{\text{cond}} \leftarrow F_{\text{tea}}(z_r, r; y_{\text{ref}})$, $v_r^{\text{uncond}} \leftarrow F_{\text{tea}}(z_r, r; \phi)$
- $v_r \leftarrow v_r^{\text{cond}} + (w_{\text{cfg}} - 1) \frac{\eta(v_r^{\text{cond}} - v_r^{\text{uncond}})}{\|v_r^{\text{cond}} - v_r^{\text{uncond}}\|}$
- $F_{\text{n2n}}, \nabla_t F_{\text{n2n}} \leftarrow \text{JVP}(F_{\theta}, (x_r, r, t; y_{\text{ref}}), (\lambda v_r, \lambda, -\gamma))$
- $g_{\text{n2n}} \leftarrow (\lambda + \gamma) \cdot \text{sg}(F_{\text{cm}}) - \lambda(v_r + (t - r)\nabla_t F_{\text{cm}}) - \gamma v_t$
- $v_{\text{n2n}}^{\text{tar}} \leftarrow \text{sg}(F_{\text{n2n}}) - w_2(r, t) \cdot g_{\text{n2n}}$
- $\mathcal{L}_{\text{n2n}} \leftarrow d_3(F_{\text{n2n}}, v_{\text{n2n}}^{\text{tar}})$ // Eq. 15
- $F'_{\text{fm}} \leftarrow F_{\theta}(x_t, t, t; y_{\text{ref}})$
- $\mathcal{L}'_{\text{fm}} \leftarrow d_2(F'_{\text{fm}}, v_t)$ // Eq. 17
- $F_{\theta}, F_{\text{ema}} \leftarrow \text{update}(F_{\theta}, \mathcal{L}_{\text{n2n}} + \mathcal{L}'_{\text{fm}})$
- end**
- $iters \leftarrow iters + 1$
- end**

we use adaptive loss weighting with power p . We set $p = 0.5$ to transform it into the Pseudo-Huber loss [51], and we find adhering to this configuration promotes training stability.

Velocity Normalization. Following [15, 39, 45], we use the velocity calculated from the CFG guidance as a reference in distillation. It can be expressed as a formula:

$$v_{\phi}^{\text{cfg}} = v_{\phi}^{\text{cond}} + (w_{\text{cfg}} - 1)(v_{\phi}^{\text{cond}} - v_{\phi}^{\text{uncond}}), \quad (18)$$

where w_{cfg} denotes CFG weights. Considering that the larger CFG weight used in some methods [11, 61] can cause over-saturation in distillation results, we perform normalization on the term $(v_{\phi}^{\text{cond}} - v_{\phi}^{\text{uncond}})$ to ensure its distribution does not deviate from v_{ϕ}^{cond} , following APG [46].

Timestep scheduling. Prior work [1, 15, 22, 24, 33] has shown that the distribution used to sample t, s in training impacts the generation quality. The sampling distribution should generally encompass a broad spectrum across

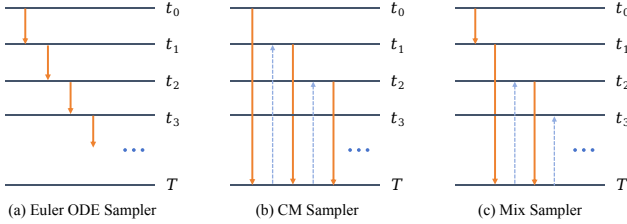


Figure 5. Illustration of Dual-End sampling, including Euler ODE sampler, CM sampler and Mix sampler.

the entire $[0, 1]$ interval. However, we find that along PF-ODE trajectories defined by the teacher model, the distillation process only needs to be carried out at specific timestep. We simply divide the interval $[0, 1]$ into N segments and perform random sampling only at the endpoints of these segments. Just using simple uniform distribution sampling can yield better results. Here we have not altered the continuous-time nature of the model. We have merely adjusted the sampling method.

Interval update policy. While the ideal approach would involve sequentially straightening the trajectories $[t, 1]$ and then $[r, t]$ in an alternating optimization manner, this poses significant practical challenges. The computational overhead of such a strategy is substantial and would prohibitively increase training time. Our simple approach is to introduce an update frequency $freq$, updating the noisy-to-noise loss every $freq$ iterations.

4.5. Sampling

As shown in Fig. 5 (a), the Euler Solver is a deterministic sampler that estimates the solution of the PF-ODE. The deterministic nature ensuring the sample semantics is preserved across NFE changes. Since the CMs relies on consistency properties to achieve few-step sampling, it cannot perform 2-8 NFE inference under Euler ODE. Fig. 5 (b) depicts the CMs sampling. At each step, it directly predicts the denoised data and then adds random noise to get midpoints, which propagates error accumulation. Through optimization focused on selected key trajectory clusters, DE-CM enables high-quality sampling in low-NFE regimes (1 and 2) while maintaining robust performance in Euler ODE solutions at higher NFE (over 16). For 4-16 NFE, we employ a mix sampling approach, as illustrated in Fig. 5 (c). Our sampling process is initiated with the Euler ODE and then followed by the CMs paradigm, as the noise-to-noisy and flow trajectories have been incorporated in optimization. This approach avoids introducing more noise and directly predicting pure noise onto the data in the early stages, effectively alleviating error accumulation.

Table 1. Class-conditional generation on ImageNet-256×256. ‘ $\times 2$ ’ indicates that CFG doubles the NFE per step. \dagger indicates distillation reproduction (250 epoch) based on our configuration.

Method	NFE (\downarrow)	#Params (\downarrow)	Time (\downarrow)	FID (\downarrow)
GAN				
BigGAN [6]	1	112M	-	6.95
GigaGAN [21]	1	569M	-	3.45
StyleGAN-XL [47]	1	166M	0.3	2.30
Masked & AR				
VQGAN [10]	256	227M	19	3.04
RQTran [25]	68	3.8B	21	3.80
MaskGIT [7]	8	227M	0.5	6.18
MAR [27]	100	945M	-	1.55
VAR-d30 [55]	10	2B	1	1.92
Diffusion & FFlow				
ADM [9]	250	280M	16	10.94
LDM-4-G [44]	250	498M	6.7	3.60
DiT-XL/2 [38]	250	675M	3.75	9.62
DiT-XL/2 ($w = 1.5$) [38]	250×2	675M	> 3.75	2.27
L-DiT [2]	250	3B	4.1	2.10
SiT-XL/2 [37]	250	675M	2.89	8.61
SiT-XL/2 ($w = 1.5$) [37]	250×2	675M	> 2.89	2.15
REPA-XL/2 ($w = 1.8$) [64]	250×2	675M	> 2.89	1.42
LightningDiT-XL/1 [61]	250	675M	2.82	2.17
LightningDiT-XL/1 ($w = 6.7$) [61]	250×2	675M	> 2.82	1.35
Consistency Model				
MeanFlow [15]	1	675M	0.011	3.43
	2		0.024	2.20
MeanFlow- \dagger [15]	1	675M	0.041	2.79
	2		0.048	1.74
IMM [66]	1×2	675M	0.057	7.77
	2×2		0.068	3.99
FACM [39]	1	675M	0.011	1.76
	4		0.047	1.56
iCT [51]	1	675M	-	34.24
	2		-	20.30
sCMs- \dagger [33]	1	675M	0.011	3.34
	2		0.024	1.94
Shortcut [13]	1	675M	0.048	10.60
	4		0.076	7.80
DE-CM (Ours)	1	675M	0.011	1.70
	2		0.024	1.33
	50		0.58	1.26

5. Experiments

5.1. Setup

For class-to-image (C2I) generation, we use ImageNet-256 × 256 datasets [8]. We implement our models in the latent space of a pre-trained VA-VAE tokenizer [61], which produces a latent dimensionality of $32 \times 16 \times 16$. Building upon the pre-trained LightningDiT [61], we introduce an additional input s to F_θ to condition the model on the right timestep. We evaluate using Fréchet Inception Distance (FID) [17] on 50K generated images. And we train the C2I model for about 3 days with learning rate 1e-4 and AdamW [32] optimizer.

For text-to-image (T2I) generation, we use 100K data from text-to-image-2M datasets [20]. We utilize the default SD3-VAE tokenizer. We leverage a reward model [60] to assess generation quality, incorporating CLIP score [41], BLIP score [26], and an overall reward score. The T2I model, initialized from Stable-Diffusion-3.5-Medium [11], is trained for approximately two days using 64 NVIDIA



Figure 6. Selected samples from DE-CM trained on ImageNet at 256×256 resolution with 2 NFE.

A100 GPUs. We adopt LoRA [19] with a rank of 64, a learning rate of 5e-4, and the AdamW optimizer.

5.2. Class-to-Image Generation

In Tab. 1 we show ImageNet 256×256 results, reporting FID scores along with the NFE (Number of Function Evaluations). Our model establishes a new state-of-the-art at 1 NFE among comparable-scale models and even surpasses the vast majority of multi-step models with just 2 NFE, demonstrating robust and superior performance. Furthermore, our model maintains stable performance at large NFE using a single set of parameters. Fig. 6 presents the visual results generated by our model using 2 NFE sampling.

5.3. Text-to-Image Generation

Fig. 7 provides a visualization of our method against competing models across various inference budgets (1, 2, 4, 32 and 50 NFE). While pre-trained models like Flux [3] and SD3.5 [11] are inherently incapable of few-step generation, existing CMs like LCM [36] and CTM [23] suffer from blurry results at low NFE and oversaturation at large NFE. Methods including PCM [57] and Hyper-SD [43], which require dedicated training for each NFE, face challenges with oversaturation and poor instruction alignment (e.g. fail to render Van Gogh style at 2 NFE). DE-CM demonstrates compelling performance, achieving appealing results in few-step inference and realistic quality at large NFE. Tab. 2 presents a quantitative evaluation using feed-

Table 2. Quantity comparison on pre-trained and CM distillation-based text-to-image model. The best and second best results of each metric are highlighted in **bold** and underline, respectively.

Method	NFE (↓)	#Params (↓)	CLIP (↑)	BLIP (↑)	Rewards (↑)
Multi-step Diffusion Models					
SD3.5-Medium [11]	4	2B	0.2395	0.4457	-1.6017
	32	2B	0.2984	0.5439	0.8028
	50	2B	<u>0.2998</u>	0.5451	0.8750
SD3.5-Large [11]	4	8B	0.2385	0.4221	-1.582
	32	8B	0.3020	0.5480	0.8153
	50	8B	0.3024	<u>0.5465</u>	0.8349
Flux.1-Dev [3]	4	12B	0.2543	0.4523	-1.2984
	32	12B	0.2929	0.5367	0.8394
	50	12B	0.2941	0.5384	<u>0.9634</u>
Few-step Diffusion Models					
SD3.5-Turbo [12]	1	8B	0.2579	0.4974	-0.8519
	2	8B	0.2590	0.4987	-0.8396
	4	8B	0.2953	<u>0.5418</u>	0.6844
	8	8B	0.2935	<u>0.5334</u>	0.6513
LCM [36]	1	2.6B	0.2508	0.4560	-1.0622
	2	2.6B	0.2937	<u>0.5202</u>	0.1441
	4	2.6B	0.2948	0.5306	0.4910
	8	2.6B	0.2993	0.5318	0.5871
CTM [23]	1	2.6B	0.2624	0.4764	-0.7639
	2	2.6B	0.2946	0.5197	0.3133
	4	2.6B	0.2986	0.5284	0.5703
	8	2.6B	0.2993	0.5278	0.6762
Hyper-SD [43]	1	2.6B	0.2939	<u>0.5161</u>	<u>0.5704</u>
	2	2.6B	0.3011	0.5168	<u>0.5399</u>
	4	2.6B	0.2949	0.5307	<u>0.7931</u>
	8	2.6B	0.3029	0.5293	<u>0.8447</u>
PCM [57]	1	2.6B	0.2726	0.4764	-0.6584
	2	2.6B	<u>0.2959</u>	0.5174	0.3454
	4	2.6B	<u>0.2981</u>	0.5265	0.6025
	8	2.6B	0.2996	0.5286	0.6195
DE-CM	1	2B	0.2996	<u>0.5398</u>	<u>0.5758</u>
	2	2B	0.2941	<u>0.5425</u>	<u>0.6853</u>
	4	2B	0.2999	<u>0.5474</u>	<u>0.8117</u>
	8	2B	<u>0.3000</u>	<u>0.5479</u>	<u>0.8671</u>
	50	2B	0.2993	0.5490	<u>0.9712</u>

back scores. Our model achieves strong performance across various metrics, notably BLIP scores, and exhibits superior sample quality universally across all NFE settings.

5.4. Ablation Studies

Tab. 3 (a)-(g) presents ablation studies under different training objectives. We can draw the following conclusions: 1) The absence of flow matching loss leads to suboptimal results due to unstable training. 2) The absence of CD loss prevents the achievement of few-step inference. 3) The absence of N2N loss affects multi-step sampling results. Lines (h)-(i) show that instantaneous velocity normalization effectively prevents oversaturation in distillation results and enhances FID performance in 1 CMs NFE and 50 ODE NFE. The results for 2 and 4 NFEs are comparable, as the inject noise process may counteract oversaturation. Lines (j)-(l) compare different time schedule designs. They reveal that confining the sampling process to specific time ranges is beneficial for the rapid distillation of high-quality models. Lines (m)-(o) demonstrate the impact of frequency selection, with excessively low values causing early training instability and high values yielding poor few-step performance. Tab. 4 shows the effectiveness of the mix sampler in alleviating error accumulation, consistently maintaining a low FID compared to ODE and CM sampler.

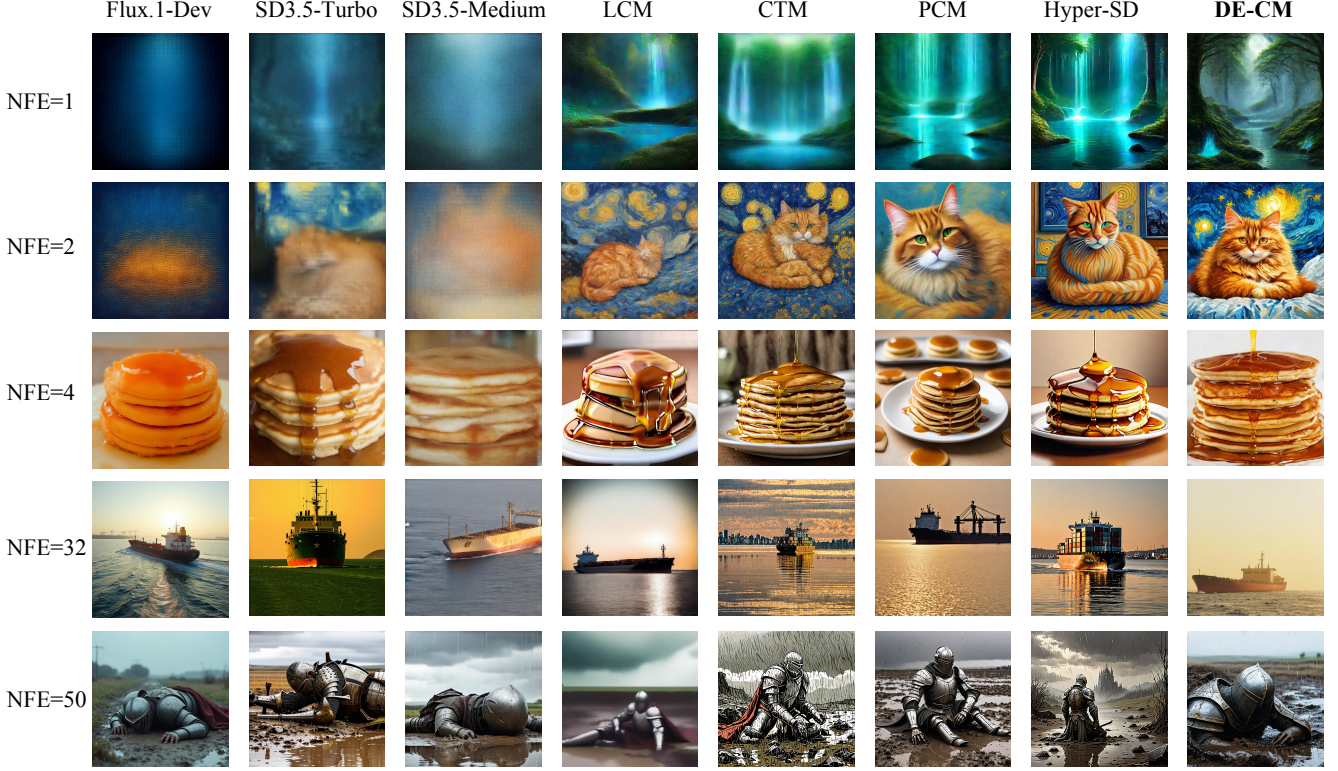


Figure 7. Qualitative visualization reveals DE-CM superiority in quality and text alignment across all NFE. Existing competing models exhibit significant step-quality trade-offs, failing at low NFE (SD3.5-Medium, FLUX.1-Dev) or producing oversaturated samples at high NFE (LCM, CTM, PCM and Hyper-SD). DE-CM maintains robust performance throughout the efficiency-quality spectrum.

Table 3. Ablation study on ImageNet-256 (FID \downarrow) analyzing the impact of training objective, velocity normalization, timestep scheduling and $freq$ across different inference steps.

Method	STEP=1	STEP=2	STEP=4	STEP=50
Training Objectives				
(a) Baseline Teacher [61]	309.51	230.79	111.59	2.77
(b) Baseline Teacher [61] ($w = 1.75$)	262.60	221.03	87.56	1.59
(c) Flow Matching (FM)	263.86	220.55	87.93	1.45
(d) CMs Distillation (CD)	3.08	2.50	2.54	6.52
(e) FM + CD	1.78	1.41	1.62	1.78
(f) FM + Noise-to-Noisy (N2N) Transmission	441.66	297.28	132.60	1.41
(g) FM + CD + N2N	1.70	1.33	1.41	1.26
Velocity Normalization.				
(h) W/ Velocity Normalization (Ours)	1.70	1.33	1.41	1.26
(i) W/O Velocity Normalization	1.75	1.30	1.43	1.35
Timestep Scheduling				
(j) uniform-with-N-seg (Ours)	1.70	1.33	1.41	1.26
(k) arctan-norm	1.74	1.36	1.62	1.45
(l) log-norm	1.83	1.45	1.67	1.41
Frequency Hyperparameter				
(m) $freq = 1$	1.72	1.48	1.77	1.45
(n) $freq = 3$ (Ours)	1.70	1.33	1.41	1.26
(o) $freq = 5$	1.74	1.34	1.52	1.37

6. Conclusion and Limitations

In this work, we propose **Dual-End Consistency Model (DE-CM)**, a novel framework that effectively addresses the dual challenges of training instability and sampling inflexibility in CMs. DE-CM strategically decomposes the

Table 4. Ablation study for sampling methods on ImageNet-256.

Sampling Method	NFE=4	NFE=8	NFE=12	NFE=16
Euler ODE Sampler	76.15	8.26	3.61	2.38
Consistency Model Sampler	1.56	2.37	3.00	3.72
Mix Sampler	1.41	1.51	1.53	1.42

PF-ODE trajectory and selects three critical sub-trajectories as optimization targets. It integrates continuous-time CMs objectives for efficient few-step distillation while employing flow matching as a boundary regularizer to ensure training stability. Furthermore, we introduce an innovative noise-to-noisy (N2N) mapping mechanism that enables flexible mapping from noise to any trajectory point, thus supporting max-sampler to alleviate error accumulation. Extensive experiments demonstrate that our method sets a new state-of-the-art FID score of 1.70 for one-step generation on the ImageNet 256×256 benchmark with 250 epoch training. Due to the incompatibility of the JVP operator with the FSDP framework and Flash Attention, the optimization process consumes a substantial amount of GPU memory, which limits the training of larger-scale models. Existing approaches try to addressed these problems, and it is hoped that more effective alternatives will emerge in the future.

References

[1] Michael S Albergo, Nicholas M Boffi, and Eric Vanden-Eijnden. Stochastic interpolants: A unifying framework for flows and diffusions. *arXiv preprint arXiv:2303.08797*, 2023. 5

[2] Alpha-VLLM. Large-dit-imagenet. <https://github.com/Alpha-VLLM/LLaMA2-Accessory/tree/main/Large-DiT-ImageNet>, 2024. 6

[3] black-forest labs. Flux.1-dev. <https://huggingface.co/black-forest-labs/FLUX.1-dev>, 2024. 7

[4] Andreas Blattmann, Tim Dockhorn, Sumith Kulal, Daniel Mendelevitch, Maciej Kilian, Dominik Lorenz, Yam Levi, Zion English, Vikram Voleti, Adam Letts, et al. Stable video diffusion: Scaling latent video diffusion models to large datasets. *arXiv preprint arXiv:2311.15127*, 2023. 1

[5] Nicholas M Boffi, Michael S Albergo, and Eric Vanden-Eijnden. Flow map matching. *arXiv preprint arXiv:2406.07507*, 2(3):9, 2024. 1

[6] Andrew Brock, Jeff Donahue, and Karen Simonyan. Large scale gan training for high fidelity natural image synthesis. *arXiv preprint arXiv:1809.11096*, 2018. 6

[7] Huiwen Chang, Han Zhang, Lu Jiang, Ce Liu, and William T Freeman. Maskgit: Masked generative image transformer. In *Proceedings of the IEEE/CVF conference on computer vision and pattern recognition*, pages 11315–11325, 2022. 6

[8] Jia Deng, Wei Dong, Richard Socher, Li-Jia Li, Kai Li, and Li Fei-Fei. Imagenet: A large-scale hierarchical image database. In *2009 IEEE conference on computer vision and pattern recognition*, pages 248–255. Ieee, 2009. 2, 6

[9] Prafulla Dhariwal and Alexander Nichol. Diffusion models beat gans on image synthesis. *Advances in neural information processing systems*, 34:8780–8794, 2021. 6

[10] Patrick Esser, Robin Rombach, and Bjorn Ommer. Taming transformers for high-resolution image synthesis. In *Proceedings of the IEEE/CVF conference on computer vision and pattern recognition*, pages 12873–12883, 2021. 6

[11] Patrick Esser, Sumith Kulal, Andreas Blattmann, Rahim Entezari, Jonas Müller, Harry Saini, Yam Levi, Dominik Lorenz, Axel Sauer, Frederic Boesel, et al. Scaling rectified flow transformers for high-resolution image synthesis. In *Forty-first international conference on machine learning*, 2024. 1, 5, 6, 7

[12] Zach Evans, CJ Carr, Josiah Taylor, Scott H Hawley, and Jordi Pons. Fast timing-conditioned latent audio diffusion. In *Forty-first International Conference on Machine Learning*, 2024. 1, 7

[13] Kevin Frans, Danijar Hafner, Sergey Levine, and Pieter Abbeel. One step diffusion via shortcut models. *arXiv preprint arXiv:2410.12557*, 2024. 6

[14] Zhengyang Geng, Ashwini Pokle, William Luo, Justin Lin, and J Zico Kolter. Consistency models made easy. *arXiv preprint arXiv:2406.14548*, 2024. 1, 3

[15] Zhengyang Geng, Mingyang Deng, Xingjian Bai, J Zico Kolter, and Kaiming He. Mean flows for one-step generative modeling. *arXiv preprint arXiv:2505.13447*, 2025. 1, 2, 3, 4, 5, 6

[16] Yi Guo, Wei Wang, Zhihang Yuan, Rong Cao, Kuan Chen, Zhengyang Chen, Yuanyuan Huo, Yang Zhang, Yuping Wang, Shouda Liu, et al. Splitmeanflow: Interval splitting consistency in few-step generative modeling. *arXiv preprint arXiv:2507.16884*, 2025. 2

[17] Martin Heusel, Hubert Ramsauer, Thomas Unterthiner, Bernhard Nessler, and Sepp Hochreiter. Gans trained by a two time-scale update rule converge to a local nash equilibrium. *Advances in neural information processing systems*, 30, 2017. 6

[18] Jonathan Ho, Ajay Jain, and Pieter Abbeel. Denoising diffusion probabilistic models. *Advances in neural information processing systems*, 33:6840–6851, 2020. 1

[19] Edward J Hu, Yelong Shen, Phillip Wallis, Zeyuan Allen-Zhu, Yuanzhi Li, Shean Wang, Lu Wang, Weizhu Chen, et al. Lora: Low-rank adaptation of large language models. *ICLR*, 1(2):3, 2022. 7

[20] Jackyhate. Text-to-image-2m. <https://huggingface.co/datasets/jackyhat/text-to-image-2M>, 2025. 6

[21] Minguk Kang, Jun-Yan Zhu, Richard Zhang, Jaesik Park, Eli Shechtman, Sylvain Paris, and Taesung Park. Scaling up gans for text-to-image synthesis. In *Proceedings of the IEEE/CVF conference on computer vision and pattern recognition*, pages 10124–10134, 2023. 6

[22] Tero Karras, Miika Aittala, Timo Aila, and Samuli Laine. Elucidating the design space of diffusion-based generative models. *Advances in neural information processing systems*, 35:26565–26577, 2022. 2, 5

[23] Dongjun Kim, Chieh-Hsin Lai, Wei-Hsiang Liao, Naoki Murata, Yuhta Takida, Toshimitsu Uesaka, Yutong He, Yuki Mitsuji, and Stefano Ermon. Consistency trajectory models: Learning probability flow ode trajectory of diffusion. *arXiv preprint arXiv:2310.02279*, 2023. 1, 2, 3, 7

[24] Nikita Kornilov, Petr Mokrov, Alexander Gasnikov, and Aleksandr Korotin. Optimal flow matching: Learning straight trajectories in just one step. *Advances in Neural Information Processing Systems*, 37:104180–104204, 2024. 5

[25] Doyup Lee, Chiheon Kim, Saehoon Kim, Minsu Cho, and Wook-Shin Han. Autoregressive image generation using residual quantization. In *Proceedings of the IEEE/CVF conference on computer vision and pattern recognition*, pages 11523–11532, 2022. 6

[26] Junnan Li, Dongxu Li, Caiming Xiong, and Steven Hoi. Blip: Bootstrapping language-image pre-training for unified vision-language understanding and generation. In *International conference on machine learning*, pages 12888–12900. PMLR, 2022. 6

[27] Tianhong Li, Yonglong Tian, He Li, Mingyang Deng, and Kaiming He. Autoregressive image generation without vector quantization. *Advances in Neural Information Processing Systems*, 37:56424–56445, 2024. 6

[28] Yaron Lipman, Ricky TQ Chen, Heli Ben-Hamu, Maximilian Nickel, and Matt Le. Flow matching for generative modeling. *arXiv preprint arXiv:2210.02747*, 2022. 1, 2

[29] Haohe Liu, Zehua Chen, Yi Yuan, Xinhao Mei, Xubo Liu, Danilo Mandic, Wenwu Wang, and Mark D Plumbley. Audi-

oldm: Text-to-audio generation with latent diffusion models. *arXiv preprint arXiv:2301.12503*, 2023. 1

[30] Ruoshi Liu, Rundi Wu, Basile Van Hoorick, Pavel Tokmakov, Sergey Zakharov, and Carl Vondrick. Zero-1-to-3: Zero-shot one image to 3d object. In *Proceedings of the IEEE/CVF international conference on computer vision*, pages 9298–9309, 2023. 1

[31] Xingchao Liu, Chengyue Gong, and Qiang Liu. Flow straight and fast: Learning to generate and transfer data with rectified flow. *arXiv preprint arXiv:2209.03003*, 2022. 1

[32] Ilya Loshchilov and Frank Hutter. Decoupled weight decay regularization. *arXiv preprint arXiv:1711.05101*, 2017. 6

[33] Cheng Lu and Yang Song. Simplifying, stabilizing and scaling continuous-time consistency models. *arXiv preprint arXiv:2410.11081*, 2024. 1, 5, 6

[34] Cheng Lu, Yuhao Zhou, Fan Bao, Jianfei Chen, Chongxuan Li, and Jun Zhu. Dpm-solver: A fast ode solver for diffusion probabilistic model sampling in around 10 steps. *Advances in neural information processing systems*, 35:5775–5787, 2022. 1

[35] Cheng Lu, Yuhao Zhou, Fan Bao, Jianfei Chen, Chongxuan Li, and Jun Zhu. Dpm-solver++: Fast solver for guided sampling of diffusion probabilistic models. *Machine Intelligence Research*, pages 1–22, 2025. 1

[36] Simian Luo, Yiqin Tan, Longbo Huang, Jian Li, and Hang Zhao. Latent consistency models: Synthesizing high-resolution images with few-step inference. *arXiv preprint arXiv:2310.04378*, 2023. 7

[37] Nanye Ma, Mark Goldstein, Michael S Albergo, Nicholas M Boffi, Eric Vanden-Eijnden, and Saining Xie. Sit: Exploring flow and diffusion-based generative models with scalable interpolant transformers. In *European Conference on Computer Vision*, pages 23–40. Springer, 2024. 6

[38] William Peebles and Saining Xie. Scalable diffusion models with transformers. In *Proceedings of the IEEE/CVF international conference on computer vision*, pages 4195–4205, 2023. 6

[39] Yansong Peng, Kai Zhu, Yu Liu, Pingyu Wu, Hebei Li, Xiaoyan Sun, and Feng Wu. Flow-anchored consistency models. *arXiv preprint arXiv:2507.03738*, 2025. 2, 5, 6

[40] Ben Poole, Ajay Jain, Jonathan T Barron, and Ben Mildenhall. Dreamfusion: Text-to-3d using 2d diffusion. *arXiv preprint arXiv:2209.14988*, 2022. 1

[41] Alec Radford, Jong Wook Kim, Chris Hallacy, Aditya Ramesh, Gabriel Goh, Sandhini Agarwal, Girish Sastry, Amanda Askell, Pamela Mishkin, Jack Clark, et al. Learning transferable visual models from natural language supervision. In *International conference on machine learning*, pages 8748–8763. PMLR, 2021. 6

[42] Aditya Ramesh, Prafulla Dhariwal, Alex Nichol, Casey Chu, and Mark Chen. Hierarchical text-conditional image generation with clip latents. *arXiv preprint arXiv:2204.06125*, 1 (2):3, 2022. 1

[43] Yuxi Ren, Xin Xia, Yanzuo Lu, Jiacheng Zhang, Jie Wu, Pan Xie, Xing Wang, and Xuefeng Xiao. Hyper-sd: Trajectory segmented consistency model for efficient image synthesis. *Advances in Neural Information Processing Systems*, 37:117340–117362, 2024. 7

[44] Robin Rombach, Andreas Blattmann, Dominik Lorenz, Patrick Esser, and Björn Ommer. High-resolution image synthesis with latent diffusion models. In *Proceedings of the IEEE/CVF conference on computer vision and pattern recognition*, pages 10684–10695, 2022. 1, 6

[45] Amirmojtaba Sabour, Sanja Fidler, and Karsten Kreis. Align your flow: Scaling continuous-time flow map distillation. *arXiv preprint arXiv:2506.14603*, 2025. 1, 2, 3, 4, 5

[46] Seyedmorteza Sadat, Otmar Hilliges, and Romann M Weber. Eliminating oversaturation and artifacts of high guidance scales in diffusion models. In *The Thirteenth International Conference on Learning Representations*, 2024. 5

[47] Axel Sauer, Katja Schwarz, and Andreas Geiger. Styleganxl: Scaling stylegan to large diverse datasets. In *ACM SIGGRAPH 2022 conference proceedings*, pages 1–10, 2022. 6

[48] Axel Sauer, Dominik Lorenz, Andreas Blattmann, and Robin Rombach. Adversarial diffusion distillation. In *European Conference on Computer Vision*, pages 87–103. Springer, 2024. 1

[49] Jascha Sohl-Dickstein, Eric Weiss, Niru Maheswaranathan, and Surya Ganguli. Deep unsupervised learning using nonequilibrium thermodynamics. In *International conference on machine learning*, pages 2256–2265. pmlr, 2015. 1

[50] Jiaming Song, Chenlin Meng, and Stefano Ermon. Denoising diffusion implicit models. *arXiv preprint arXiv:2010.02502*, 2020. 1

[51] Yang Song and Prafulla Dhariwal. Improved techniques for training consistency models. *arXiv preprint arXiv:2310.14189*, 2023. 1, 3, 5, 6

[52] Yang Song and Stefano Ermon. Generative modeling by estimating gradients of the data distribution. *Advances in neural information processing systems*, 32, 2019. 1

[53] Yang Song, Jascha Sohl-Dickstein, Diederik P Kingma, Abhishek Kumar, Stefano Ermon, and Ben Poole. Score-based generative modeling through stochastic differential equations. *arXiv preprint arXiv:2011.13456*, 2020. 1

[54] Yang Song, Prafulla Dhariwal, Mark Chen, and Ilya Sutskever. Consistency models. 2023. 1, 2, 3

[55] Keyu Tian, Yi Jiang, Zehuan Yuan, Bingyue Peng, and Liwei Wang. Visual autoregressive modeling: Scalable image generation via next-scale prediction. *Advances in neural information processing systems*, 37:84839–84865, 2024. 6

[56] Team Wan, Ang Wang, Baole Ai, Bin Wen, Chaojie Mao, Chen-Wei Xie, Di Chen, Feiwu Yu, Haiming Zhao, Jianxiao Yang, Jianyuan Zeng, Jiayu Wang, Jingfeng Zhang, Jingen Zhou, Jinkai Wang, Jixuan Chen, Kai Zhu, Kang Zhao, Keyu Yan, Lianghua Huang, Mengyang Feng, Ningyi Zhang, Pandeng Li, Pingyu Wu, Ruihang Chu, Ruili Feng, Shiwei Zhang, Siyang Sun, Tao Fang, Tianxing Wang, Tianyi Gui, Tingyu Weng, Tong Shen, Wei Lin, Wei Wang, Wei Wang, Wenmeng Zhou, Wente Wang, Wenting Shen, Wenyuan Yu, Xianzhong Shi, Xiaoming Huang, Xin Xu, Yan Kou, Yangyu Lv, Yifei Li, Yijing Liu, Yiming Wang, Yingya Zhang, Yitong Huang, Yong Li, You Wu, Yu Liu, Yulin Pan, Yun Zheng, Yuntao Hong, Yupeng Shi, Yutong Feng, Zeyinzi Jiang, Zhen Han, Zhi-Fan Wu, and Ziyu Liu. Wan: Open and advanced large-scale video generative models. *arXiv preprint arXiv:2503.20314*, 2025. 1

[57] Fu-Yun Wang, Zhaoyang Huang, Alexander Bergman, Dazhong Shen, Peng Gao, Michael Lingelbach, Keqiang Sun, Weikang Bian, Guanglu Song, Yu Liu, et al. Phased consistency models. *Advances in neural information processing systems*, 37:83951–84009, 2024. 7

[58] Zhengyi Wang, Cheng Lu, Yikai Wang, Fan Bao, Chongxuan Li, Hang Su, and Jun Zhu. Prolificdreamer: High-fidelity and diverse text-to-3d generation with variational score distillation. *Advances in neural information processing systems*, 36:8406–8441, 2023. 1

[59] Zhangkai Wu, Xuhui Fan, Hongyu Wu, and Longbing Cao. Traflow: Trajectory distillation on pre-trained rectified flow. *arXiv preprint arXiv:2502.16972*, 2025. 2, 4

[60] Jiazheng Xu, Xiao Liu, Yuchen Wu, Yuxuan Tong, Qinkai Li, Ming Ding, Jie Tang, and Yuxiao Dong. Imagereward: learning and evaluating human preferences for text-to-image generation. In *Proceedings of the 37th International Conference on Neural Information Processing Systems*, pages 15903–15935, 2023. 6

[61] Jingfeng Yao, Bin Yang, and Xinggang Wang. Reconstruction vs. generation: Taming optimization dilemma in latent diffusion models. In *Proceedings of the Computer Vision and Pattern Recognition Conference*, pages 15703–15712, 2025. 5, 6, 8

[62] Tianwei Yin, Michaël Gharbi, Taesung Park, Richard Zhang, Eli Shechtman, Fredo Durand, and Bill Freeman. Improved distribution matching distillation for fast image synthesis. *Advances in neural information processing systems*, 37:47455–47487, 2024. 1

[63] Tianwei Yin, Michaël Gharbi, Richard Zhang, Eli Shechtman, Fredo Durand, William T Freeman, and Taesung Park. One-step diffusion with distribution matching distillation. In *Proceedings of the IEEE/CVF conference on computer vision and pattern recognition*, pages 6613–6623, 2024. 1

[64] Sihyun Yu, Sangkyung Kwak, Huiwon Jang, Jongheon Jeong, Jonathan Huang, Jinwoo Shin, and Saining Xie. Representation alignment for generation: Training diffusion transformers is easier than you think. *arXiv preprint arXiv:2410.06940*, 2024. 6

[65] Lvmin Zhang, Anyi Rao, and Maneesh Agrawala. Adding conditional control to text-to-image diffusion models. In *Proceedings of the IEEE/CVF international conference on computer vision*, pages 3836–3847, 2023. 1

[66] Linqi Zhou, Stefano Ermon, and Jiaming Song. Inductive moment matching. *arXiv preprint arXiv:2503.07565*, 2025. 1, 6